

The structure of Au_6Y^+ in the gas phase†

Ling Lin,^{ab} Pieterjan Claes,^{bc} Tibor Höltzl,^{ab} Ewald Janssens,^{bc} Torsten Wende,^d Risshu Bergmann,^d Gabriele Santambrogio,^e Gerard Meijer,^d Knut R. Asmis,^{*d} Minh Tho Nguyen^{*ab} and Peter Lievens^{*bc}

Received 17th June 2010, Accepted 20th August 2010

DOI: 10.1039/c0cp00911c

The geometric and electronic structure of the Au_6Y^+ cation is studied by gas phase vibrational spectroscopy combined with density functional theory calculations. The infrared photodissociation spectrum of $\text{Au}_6\text{Y}^+\cdot\text{Ne}$ is measured in the 95–225 cm^{-1} energy range and exhibits two characteristic absorption bands at 181 cm^{-1} and 121 cm^{-1} . Based on DFT/BP86 quantum chemical calculations, the infrared spectrum is assigned to the lowest energy species found, an eclipsed C_{3v} geometry. The 3D structure of Au_6Y^+ is considerably different from those previously found for both the neutral Au_6Y (quasi-planar circular geometry) and the anionic Au_6Y^- (planar D_{6h} symmetry). The different geometries are related to different electronic structures in agreement with 2D and 3D phenomenological shell models for metal clusters.

Gold clusters have attracted continuing attention, in part due to their potential applications in several areas, for example as efficient catalysts for chemical reactions.¹ The geometry and the dimensionality (planar or three-dimensional) of small Au_n clusters are closely linked to their catalytic activities.^{2,3} Small neutral Au_n clusters prefer planar shapes in their lowest-energy structures and a 2D–3D transition occurs at size $n \approx 12$.^{4,5} The preference for 2D forms has been interpreted as a consequence of relativistic effects of the gold element.^{6,7} Removal or addition of an electron from neutral gold clusters modifies their structure, but they remain planar up to $n \approx 7$ (Au_n^+) and $n \approx 11$ (Au_n^-), respectively.^{8–10} Thus in small gold clusters, electron excess tends to favor planar structures up to larger cluster sizes than electron deficiency. Recent review articles give a comprehensive overview of the current knowledge on the structures of neutral and ionic gold clusters.^{6,11–13}

It is well established that doping a cluster by another element can modify cluster properties such as its shape, electronic, or optical properties.^{14–22} For example, small Au_nS clusters were predicted to adopt a 3D structure from $n = 6$.¹⁸ For Au_nSi , density functional theory (DFT) showed that 3D

structures start already from $n = 3$, which is accounted for by the strong directional covalent bonding resulting from a significant contribution of the p electrons of Si.²¹ Within this series, Au_4Si adopts a T_d structure and shows extraordinary stability.¹⁶ In the series of Au_5M with $M = \text{Na}, \text{Mg}, \text{Al}, \text{Si},$ or P , the dopant atoms with s valence electrons (Na, Mg) were predicted to have planar structures similar to Au_6 , while those with p valence electrons ($\text{Al}, \text{Si}, \text{P}$) result in non-planar structures.¹⁹ Recently it was shown that also isoelectronic substitution of Au by Ag or Cu in Au_n^- shifts the 2D to 3D structural transition to smaller sizes.²² A systematic theoretical study on Au_nZn ($n \leq 6$)¹⁴ showed that all the lowest-energy isomers are planar, and structurally resemble the pure Au_{n+1} clusters. The enhanced stability of the bimetallic Au_5Zn^+ cation is the result of its σ -aromatic nature.¹⁵ For Au_nM with $n = 2–7$ and $M = \text{Ni}, \text{Pd},$ and Pt , the planar structures are again favored for all clusters studied, except Au_7Ni , for which the most stable 3D structure turns out to be almost degenerate with its corresponding 2D form.¹⁷ Overall, these studies, among many others, consistently show that doping is indeed a powerful way of tuning the properties of gold clusters.

Previous studies on the neutral Au_6M and anionic Au_6M^- clusters with $M = \text{Ti}, \text{V}, \text{Cr}$ pointed out that all these clusters prefer planarity. The transition metal atom is located at the center of a Au_6 ring, and its magnetic moment is not quenched by the nonmagnetic gold host.²³ The stability of the quartet state and the D_{6h} point group of Au_6Mn was explained using an extension of the phenomenological shell model for metal clusters, which also provides a consistent rationalization for the observed variation of the electronic state of the whole series of 3d transition metal doped Au_6M .²⁴

Recently, we reported that the neutral yttrium-doped Au_6Y cluster has a quasi-planar structure and a fluxional behaviour.^{25,26} The geometry was assigned by comparing the experimental infrared photodissociation (IRPD) spectrum with the results from quantum chemical calculations. The planar transition state for rearrangement lies only a few kJ mol^{-1} above the 3D C_{2v} equilibrium structures, resulting in fluxional behavior at finite temperatures and line broadening in the experimental IRPD spectra. The quantum chemical calculations also showed that upon attachment of an electron to Au_6Y , the resulting Au_6Y^- anion adopts a fully planar, highly symmetric D_{6h} structure. The anion was characterized as a new bimetallic six-membered cyclic species featuring σ -aromaticity.²⁵ The geometry of the corresponding Au_6Y^+ cation, although its existence as a stable gas phase species was established already quite some time ago,²⁷ has not been investigated yet. Indeed Au_6Y^+ has been observed in large abundances relative to neighboring sizes in mass spectrometric

^a Department of Chemistry, Katholieke Universiteit Leuven, B-3001 Leuven, Belgium. E-mail: minh.nguyen@chem.kuleuven.be

^b INPAC-Institute for Nanoscale Physics and Chemistry, Katholieke Universiteit Leuven, B-3001 Leuven, Belgium

^c Laboratory of Solid State Physics and Magnetism, Katholieke Universiteit Leuven, B-3001 Leuven, Belgium. E-mail: peter.lievens@fys.kuleuven.be

^d Fritz-Haber-Institut der Max-Planck-Gesellschaft, Faradayweg 4–6, D-14195 Berlin, Germany. E-mail: asmis@fhi-berlin.mpg.de

^e East Tokyo Laboratory, Genesis Research Institute, Inc., 717-86 Futamata, Ichikawa 272-0001, Japan

† Electronic supplementary information (ESI) available: Vibrational spectra of $\text{Au}_6\text{Y}^+\cdot\text{Ne}$, NBO charges and Electron Localizability Indicator (ELI-D) of Au_6Y^+ , and movies illustrating the motions of Au_6Y^+ . See DOI: 10.1039/c0cp00911c

studies, suggesting an enhanced stability.^{27,28} However, the origin of this stability as well as the electronic and geometric structure of Au_6Y^+ have not been addressed so far.

As part of our continued interest in metal doped gold clusters, we combine experimental and theoretical approaches to characterize the structure of Au_6Y^+ in the present study. First, we show the experimental IRPD spectrum of $\text{Au}_6\text{Y}^+\cdot\text{Ne}$. Then the cluster geometry is assigned with the aid of quantum chemical calculations. Finally, the geometric and electronic structures of Au_6Y^+ are compared with those of its neutral and anionic counterparts and differences among each other are discussed on the basis of the phenomenological shell model.

The IRPD experiments are performed with a tandem mass spectrometer-ion trap instrument,^{29,30} which is coupled to a beamline of the Free Electron Laser for Infrared eXperiments (FELIX) at the FOM Institute for Plasma Physics Rijnhuizen.³¹ Binary clusters are produced with a pulsed (10 Hz) dual-target dual-laser vaporization source.³² Following vaporization, the plasma containing gold and yttrium atoms is entrained in a short pulse of helium carrier gas and expansion through a condensation channel triggers cluster formation. The molecular beam passes a 4 mm diameter skimmer and the cationic clusters are collimated in a He-filled, radio frequency (RF) multipole ion guide. Next, Au_6Y^+ ions (1271 amu) are mass-selected by a quadrupole mass filter and guided into a cryogenically cooled RF ring electrode trap filled with a continuous flow of Ne. Through many collisions with the Ne buffer gas, the ions are decelerated, trapped, and thermalized. At sufficiently low trap temperatures, 19 K for the present experiments, $\text{Au}_6\text{Y}^+\cdot\text{Ne}$ complexes are efficiently formed by three-body collisions.^{33,34} Given a calculated neon binding energy of ~ 0.12 eV at the Y site for all Au_6Y^+ isomers considered, the absorption of a few IR photons (5 photons at 181 cm^{-1} and 8 photons at 121 cm^{-1}) by the weakly-bound cluster–rare gas complex is sufficient for vibrational predissociation to occur. IRPD spectra are obtained by photoexcitation of the trapped ions with pulsed radiation from FELIX, which is operated at 5 Hz and applied collinear to the ion trap main axis. Directly after FELIX fires, all ions are extracted from the trap into a time-of-flight mass spectrometer. IRPD spectra are measured in the difference mode of operation (laser on–laser off) by monitoring the changes in the $\text{Au}_6\text{Y}^+\cdot\text{Ne}$ (depletion) and Au_6Y^+ (formation) signals. IRPD spectra are measured in the $95\text{--}225\text{ cm}^{-1}$ range with a step size of $0.5\text{ }\mu\text{m}$. The FELIX beam intensity was appropriately attenuated in order to avoid saturation. We used typical energies of 14 mJ and a bandwidth of $3\text{--}4\text{ cm}^{-1}$, which is the full width at half maximum (FWHM) of the central wavelength.

Fig. 1 depicts the normalized IRPD spectrum of $\text{Au}_6\text{Y}^+\cdot\text{Ne}$ in the $95\text{--}225\text{ cm}^{-1}$ energy range. The spectrum shows two distinct and characteristic peaks centered at 181 cm^{-1} and 121 cm^{-1} with a FWHM of around 5 cm^{-1} , which is comparable to the spectral bandwidth of the FELIX pulse.

Quantum chemical computations are carried out with the Gaussian 03 suite of programs.³⁵ Geometry optimizations, harmonic frequency computations, and single-point energy calculations are performed using the pure BP86 density functional^{36,37} in conjunction with the cc-pVTZ (for Ne),

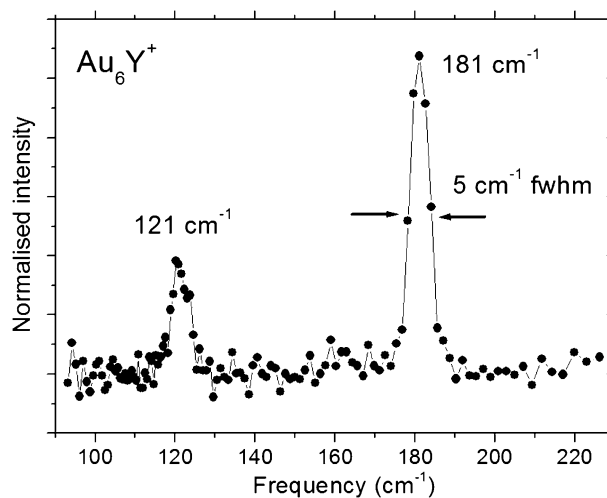


Fig. 1 Experimental IRPD spectrum of $\text{Au}_6\text{Y}^+\cdot\text{Ne}$ in the range from 95 to 225 cm^{-1} (110 to $45\text{ }\mu\text{m}$). The plotted values are normalized for the sum of parent ($\text{Au}_6\text{Y}^+\cdot\text{Ne}$) and fragment (Au_6Y^+) intensities, $I_{\text{Au}_6\text{Y}^+\cdot\text{Ne}}/(I_{\text{Au}_6\text{Y}^+} + I_{\text{Au}_6\text{Y}^+\cdot\text{Ne}})$. The parent and the fragment ion intensities were measured as the difference between the averaged signals with laser on and laser off to minimize the influence of cluster production fluctuations.

and cc-pVDZ-PP (for Au and Y) basis sets, where PP stands for pseudopotential.^{38–40} The vibrational frequencies are scaled according to a fitting equation ($\tilde{\nu} = 22\text{ cm}^{-1} + \tilde{\nu}_{\text{calc.}} \times 0.94$) derived in a previous study for the neutral Au_nY ($n = 1\text{--}9$).²⁶ The calculated stick spectra are folded with a Gaussian line width function of 5 cm^{-1} FWHM for ease of comparison with the experimental spectra. The electron localizability indicator (ELI-D)^{41,42} is computed using the Dgrid 4.1 program,⁴³ while the NBO 3.1 code is used for natural orbital analysis.⁴⁴ As an alternative way to investigate the electronic structure of the clusters, the total and partial densities of states (DOS) are calculated with the Pymolize program.⁴⁵

Fig. 2 displays the four lowest-lying energy minima that were found (**iso-1** to **-4**). For comparison of Au_6Y^+ with the isoelectronic Cu_6Sc^+ , also a tricapped tetrahedral C_{3v} isomer is shown (**iso-5**). This isomer is the ground state of Cu_6Sc^+ ,⁴⁶ but it is a high energy isomer on the Au_6Y^+ potential energy surface. The DFT computations yield the C_{3v} structure **iso-1** as the lowest-energy structure. It is 0.51 eV more stable than the tricapped tetrahedron C_{3v} form **iso-5**. In fact **iso-1** and **iso-5** correspond to two distinct conformers, **iso-1** has an eclipsed conformation and **iso-5** is its staggered counterpart. The relative energy of **iso-2** with respect to **iso-1** is only $+0.02\text{ eV}$ (including zero-point energy corrections) and the relative energy ordering even inverts if free energy corrections are considered (in that case **iso-2** is 0.02 eV more stable than **iso-1**). These energy differences are well below the DFT uncertainties and thus theory alone does not allow assigning the ground state geometry.

As can be seen in Fig. 2, the simulated linear absorption spectrum of **iso-1** agrees very well with IRPD spectrum. It displays an absorption band at 183 cm^{-1} and a less intense band centered at 123 cm^{-1} , while the experimental spectrum (bottom trace) shows bands at 181 cm^{-1} and 121 cm^{-1} with similar intensity ratio. On the other hand the simulated

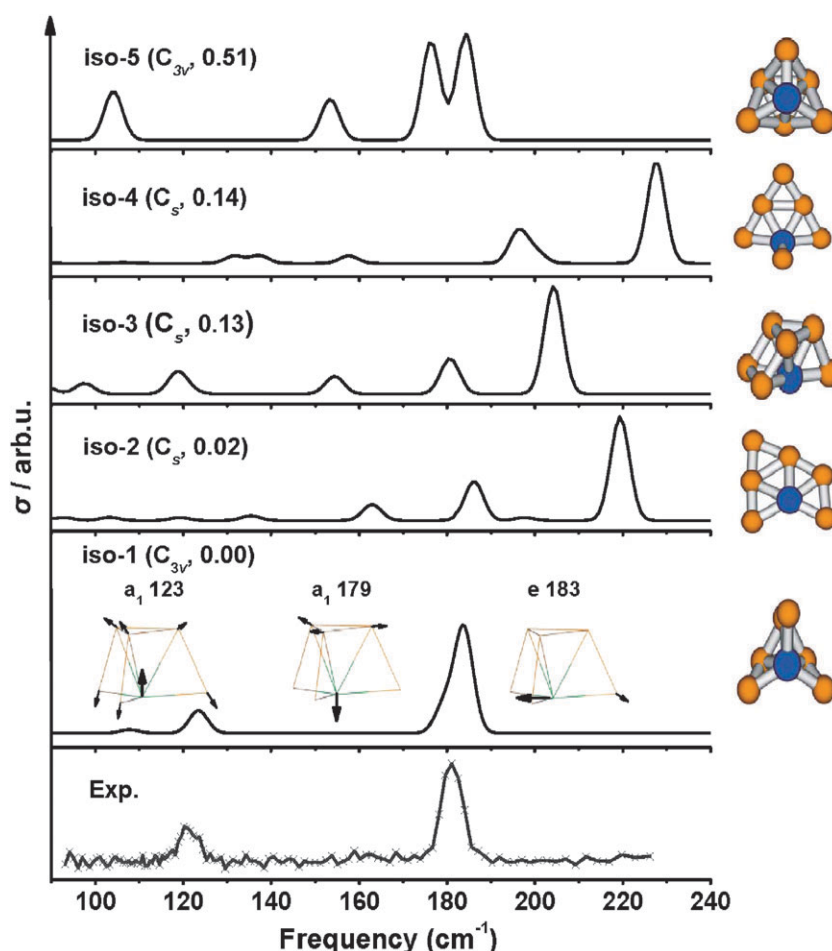


Fig. 2 Comparison of the calculated (BP86/cc-pVDZ-PP) vibrational spectra of five low-lying Au_6Y^+ isomers (relative energies are given in eV) with the experimental IRPD spectrum. The normal modes accounting for the three bands of the lowest-energy isomer are shown. The modes are labelled with their symmetry and corresponding frequency in cm^{-1} . Movies illustrating the motions are given in the ESI†.

absorption spectrum of **iso-2** does not match the experiment at all (neither do **iso-3**, **iso-4**, and **iso-5**). This is a strong argument to claim that **iso-1** is the most abundant isomer of Au_6Y^+ in the molecular beam. Vibration spectra are a fingerprint of the geometry; different isomers of the same cluster typically have very different vibration spectra. Indeed, infrared spectroscopy has been demonstrated to be a very sensitive technique, which in combination with DFT allows unambiguous assignment of ground state geometries of mass-selected cluster ions in the gas phase.⁴⁷ The presence of small fractions of other isomers (such as **iso-2**) can strictly not be excluded because (i) the IRPD experiments are performed on the $\text{Au}_6\text{Y}^+\cdot\text{Ne}$ complexes and different isomers can have a different efficiency for complex formation, and (ii) the noise level is not zero, so the presence of absorption bands originating from weak traces of other isomers might be hidden in the experimental background. Nonetheless given that (i) the intensities of Au_6Y^+ and $\text{Au}_6\text{Y}^+\cdot\text{Ne}$ in the trap (without FELIX irradiation) are comparable and thus a major fraction of the clusters form Ne complexes, (ii) the depletion of the complexes reaches up to 60% (at the 181 cm^{-1} band), and (iii) the IRPD spectra have a good signal-to-noise ratio, we conclude that **iso-1** is by far the most abundant isomer of Au_6Y^+ in the molecular beam.

Each of the normal modes of **iso-1** associated with the observed infrared bands involves a motion of the dopant (see the movies in the ESI†). The 123 cm^{-1} band is mainly due to Y-atom displacement (see Movie S1, ESI†), whereas the 183 cm^{-1} band comprises three Au–Y stretching modes, one at 179 cm^{-1} (see Movie S2, ESI†) and two degenerate modes at 183 cm^{-1} (see Movie S3, ESI†). The calculated spectrum of $\text{Au}_6\text{Y}^+\cdot\text{Ne}$ is shown in Fig. S1 (ESI†) and it is similar to that of Au_6Y^+ .

Fig. 3 displays the far-IR spectra of the most stable cations Au_nY^+ ($n = 1-6$), along with the optimized cluster structures, calculated using the same method. For all sizes, the most intense band is the one with the highest frequency, which is centered at 227, 245, 235, 210, 212, and 183 cm^{-1} for $n = 1, 2, 3, 4, 5,$ and 6 , respectively. These frequencies correspond to Y–Au stretching modes of the bond(s) between Y and the lowest coordinated Au atom(s). The overall decrease of the frequency of this most intense band with increasing size n is related to the increased coordination of the Y atom and the corresponding enhanced delocalization of the bonding charge.

The geometric structure of the cationic Au_6Y^+ differs considerably from that of its neutral counterpart.^{25,26} The latter is characterized by several degenerate symmetry-equivalent

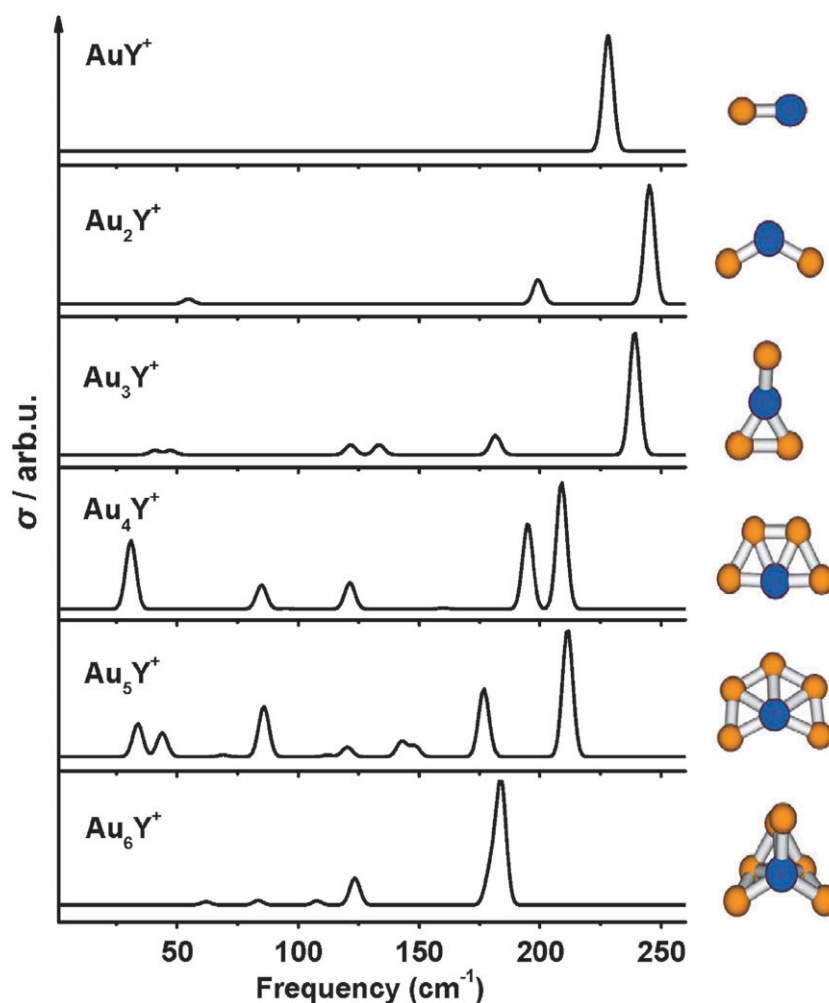


Fig. 3 Vibrational spectra of the ground state isomers of Au_nY^+ ($n = 1-6$) calculated at the BP86/cc-pVDZ-PP level.

structures, which are connected by very low energy barriers resulting in a fluxional quasi-planar shape that induces, in turn, a strong line broadening of its IRPD bands.^{25,26} The cationic Au_6Y^+ , on the contrary, exhibits a rigid 3D structure and its IRPD spectrum does not suffer from line broadening. The geometry of Au_6Y^+ also differs from that of the isovalent Cu_6Sc^+ .⁴⁶ Both have a 3D geometry with the dopant atom occupying a highly coordinated position, but Cu_6Sc^+ has a tricapped-tetrahedron shape, analogous to **iso-5**, whereas Au_6Y^+ has an eclipsed C_{3v} symmetry. The structural difference between Cu_6Sc^+ and Au_6Y^+ clusters could arise from distinct atomic sizes and relativistic effects in Au inducing a stronger s(Au)-d(Y) hybridization (to be discussed elsewhere).

Natural orbital analysis of Au_6Y^+ shows that the Y center carries a positive charge of +1.04 electrons. The Au atoms in the small gold triangle are slightly positively charged (+0.13 electron), whereas those in the large gold triangle are slightly negatively charged (-0.14 electron) (Fig. S2 in ESI†). The yttrium atom has a $5s(0.61)4d(1.24)5p(0.08)$ electron configuration. To probe the electronic structure of Au_6Y^+ , the total and partial (projected onto the local s-like atomic orbitals) densities of states are analyzed and given in Fig. 4. The molecular orbitals (MOs) with high contributions from the valence s atomic orbitals (AOs) are assigned on the basis of

similarities between their shape and the wave functions of an electron in a spherically symmetric potential.⁴⁸ These MOs are labeled according to the notations of the phenomenological shell model as shown in Fig. 5a.

The phenomenological shell model basically assumes that the valence electrons are delocalized over the whole cluster. In its simplest version, the electrons are treated as moving in a simple mean-field potential, whereas the nuclei only contribute a constant background.⁴⁹ Accordingly, the valence s-like AOs form MOs having shapes similar to that of the s, p, and d AOs. These MOs are labeled hereafter by capital S, P, and D letters. Enhanced stability of metal clusters is expected if the number of delocalized electrons corresponds to a closed electronic structure, *i.e.*, filled shells of electrons. In the case of spherical arrangement of atoms a shell closure occurs if the cluster has 2, 8, 20... itinerant electrons. $(1S)^2$, $(1S)^2(1P)^6$, and $(1S)^2(1P)^6(2S)^2(1D)^{10}$ electron configurations correspond to these magic numbers, respectively. Each electronic shell $(NL)^x$ is characterized by a radial quantum number N ($N = 1, 2, 3...$) and an angular quantum number L ($L = S, P, D...$). The superscript x indicates the occupancy of the MO. This shell model was successful in explaining the size dependency of several properties of bare gold clusters.¹¹ An extension of the shell model towards planar metal clusters

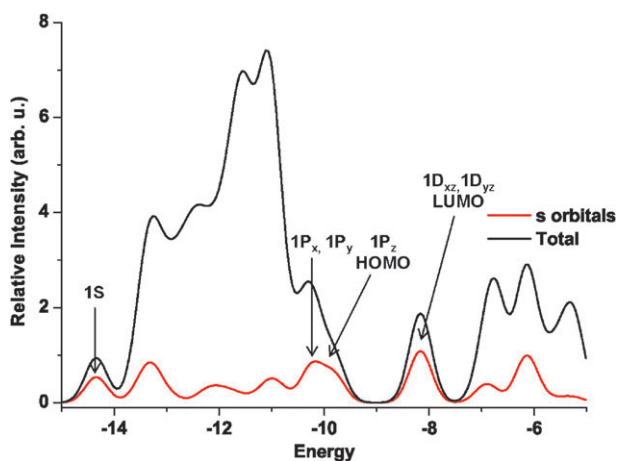


Fig. 4 Total and partial (only s-type AOs) densities of states of the most stable Au_6Y^+ cluster (**iso-1**) with the assignment of the MOs with high contributions from the valence s-like AOs on the basis of similarities with wave functions of an electron in a spherical symmetric potential using the nomenclature of the phenomenological shell model.

showed that the number of electrons yielding closed electronic shells depends on the shape of the cluster.⁵⁰ In the case of triangular or rectangular clusters, enhanced stabilities are

expected for structures having 2, 6, 8, 12, 16, or 20 delocalized s-type electrons, whereas the number of these electrons is 2, 6, 10, 12, 16, or 20 for clusters with a circular shape.

Au_6Y^+ has eight delocalized electrons from the six Au ($6s^1$) and one Y ($4d^15s^2$) atoms minus one electron due to the cationic state of the cluster. These eight electrons can be organized in a closed shell $(1S)^2(1P)^6$ configuration if the cluster has a spherical shape.⁴⁹ However, due to the relatively small size of the cluster, a distortion of the spherical geometry is expected. Indeed, with a diameter of about 2.9 Å and a height of about 2.5 Å, Au_6Y^+ has an oblate shape, which results in a lifting of the degeneracy of the $1P_x$, $1P_y$, and $1P_z$ subshells.⁵¹ Due to the C_{3v} symmetry of the cluster, the 1P orbitals are decomposed into orbitals belonging to the E (degenerate $1P_x$ and $1P_y$) and A_1 ($1P_z$) irreducible representations of the C_{3v} point group. A molecular orbital analysis of the clusters indeed shows that the electronic structure of Au_6Y^+ corresponds to a closed $(1S)^2(1P_x, 1P_y)^4(1P_z)^2$ configuration. The splitting of the P levels ($1P_z$ orbital is 0.43 eV higher in energy than the $1P_x$ and $1P_y$ levels) is in line with the results of the phenomenological shell model for oblate shaped species.⁵¹

Electron attachment to the cationic Au_6Y^+ yields the neutral Au_6Y . In a spherical geometry, the ninth valence

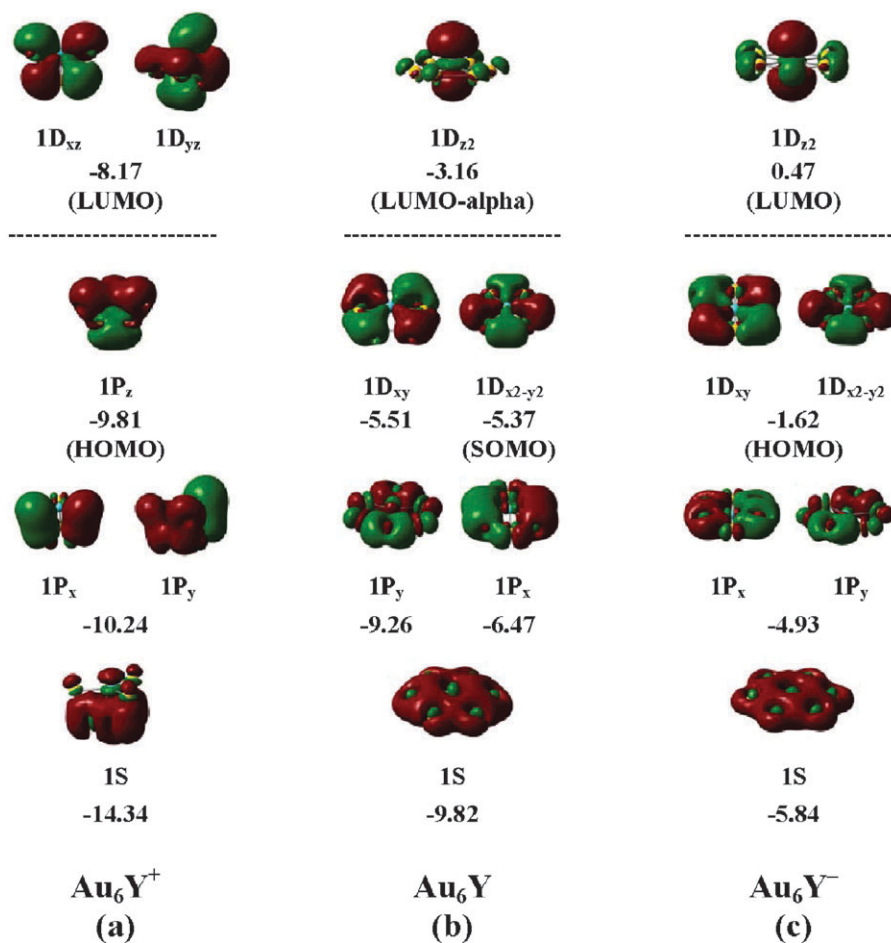


Fig. 5 The shape and energies (in eV; for Au_6Y only the energies of the MOs with alpha electrons are provided) of MOs of (a) Au_6Y^+ , (b) Au_6Y , and (c) Au_6Y^- ,²⁵ with an assignment based on the phenomenological shell model. All MOs are doubly occupied, except LUMO and SOMO of Au_6Y .

electron should occupy the empty 1D orbital to get an open shell $(1S)^2(1P)^6(1D)^1$ configuration. However, as demonstrated by an earlier combined infrared spectroscopy and density function theory study, Au_6Y prefers a quasi-planar circular geometry.^{25,26} Therefore, the MOs corresponding to the phenomenological shell model $1P_z$ will be unoccupied, whereas the $1D_{xy}$ and $1D_{x^2-y^2}$ orbitals are occupied with two and one electrons, respectively. These orbitals in the gap region are depicted in Fig. 5b. The Au_6Y neutral cluster is thus an open shell system and Jahn–Teller instability prevents a symmetric planar ring structure. However, upon addition of another electron, yielding Au_6Y^- , the $1D_{x^2-y^2}$ becomes doubly occupied (see Fig. 5c). The Au_6Y^- cluster has 10 delocalized electrons, which in a planar symmetry correspond to a closed shell $(1S)^2(1P_x, 1P_y)^4(1D_{xy}, 1D_{x^2-y^2})^4$ configuration.

The closed shell structure of Au_6Y^+ and Au_6Y^- is reflected in their high HOMO–LUMO gaps of 1.63 eV and 2.07 eV, respectively; HOMO stands for highest occupied molecular orbital and LUMO stands for lowest unoccupied molecular orbital. The open shell Au_6Y , on the other hand, has a SOMO (alpha)-LUMO (beta) gap of 0.25 eV only; SOMO denotes singly occupied molecular orbital.

In summary, we have investigated both experimentally and computationally the geometric, vibrational, and electronic properties of the yttrium-doped gold species Au_6Y^+ containing eight delocalized electrons. The experimental IRPD spectrum of $Au_6Y^+ \cdot Ne$ can be explained by DFT calculations. The observed absorption bands at 181 cm^{-1} and 121 cm^{-1} are associated to motions of the Y dopant. The lowest energy Au_6Y^+ cluster has a 3D oblate eclipsed C_{3v} shape, in contrast to the quasi-planar C_{2v} and planar D_{6h} shapes for the neutral and anionic counterparts, respectively. The cationic Au_6Y^+ possesses a $1S^2(1P_x, 1P_y)^4 1P_z^2$ closed shell electronic structure and the contributions of local s-like electrons are predominant in the chemical bond formation. Comparing Au_6Y^+ (8 s-like valence electrons) with Au_6Y^- (10 s-like valence electrons), a transition from a 3D to a 2D geometry is observed as the most probable structure. The cluster thus seems to seek the shell closing that is closest or easiest to match, even if this implies a change of the dimensionality.

Acknowledgements

The authors gratefully acknowledge the support of the Stichting voor Fundamenteel Onderzoek der Materie (FOM) in providing the required beam time on FELIX and highly appreciate the skillful assistance of the FELIX staff. This work is supported by the Fund for Scientific Research—Flanders (FWO), the K.U.Leuven Research Council (BOF, GOA and IDO programs), the Belgian Interuniversity Attraction Poles (IAP) research program, the German Research Foundation within the dedicated research center SFB-546 and the European Community's Seventh Framework Programme (FP7/2007-2013) under grant agreement no. 226716. LL and TH thank INPAC for financial support, and PC thanks the Institute for the Promotion of Innovation through Science and Technology in Flanders (IWT-Vlaanderen) for a doctoral scholarship.

References

- S. Chrétien, S. K. Buratto and H. Metiu, *Curr. Opin. Solid State Mater. Sci.*, 2007, **11**, 62.
- B. Yoon, H. Häkkinen, U. Landman, A. S. Wörz, J. M. Antonietti, S. Abbet, K. Judai and U. Heiz, *Science*, 2005, **307**, 403.
- A. A. Herzing, C. J. Kiely, A. F. Carley, P. Landon and G. J. Hutchings, *Science*, 2008, **321**, 1331.
- X. B. Li, H. Y. Wang, X. D. Yang, Z. H. Zhu and Y. J. Tang, *J. Chem. Phys.*, 2007, **126**, 084505.
- E. M. Fernández, J. M. Soler, I. L. Garzón and L. C. Balbás, *Phys. Rev. B*, 2004, **70**, 165403.
- P. Pykkö, *Angew. Chem.*, 2004, **116**, 4512 (*Angew. Chem., Int. Ed.*, 2004, **43**, 4412).
- H. Häkkinen, M. Moseler and U. Landman, *Phys. Rev. Lett.*, 2002, **89**, 033401.
- S. Gilb, P. Weis, F. Furche, R. Ahlrichs and M. M. Kappes, *J. Chem. Phys.*, 2002, **116**, 4094.
- M. P. Johansson, A. Lechtken, D. Schooss, M. M. Kappes and F. Furche, *Phys. Rev. A*, 2008, **77**, 053202.
- W. Huang and L. S. Wang, *Phys. Rev. Lett.*, 2009, **102**, 153401.
- H. Häkkinen, *Chem. Soc. Rev.*, 2008, **37**, 1847.
- P. Pykkö, *Chem. Soc. Rev.*, 2008, **37**, 1967.
- D. Schoos, P. Weis, O. Hampe and M. M. Kappes, *Philos. Trans. R. Soc., A*, 2010, **368**, 1211.
- H. Tanaka, S. Neukermans, E. Janssens, R. E. Silverans and P. Lievens, *J. Chem. Phys.*, 2003, **119**, 7115.
- H. Tanaka, S. Neukermans, E. Janssens, R. E. Silverans and P. Lievens, *J. Am. Chem. Soc.*, 2003, **125**, 2862.
- B. Kiran, X. Li, H. J. Zhai, L. F. Cui and L. S. Wang, *Angew. Chem., Int. Ed.*, 2004, **43**, 2125.
- D. W. Yuan, Y. Wang and Z. Zeng, *J. Chem. Phys.*, 2005, **122**, 114310.
- C. Majumder and S. K. Kulshreshtha, *Phys. Rev. B*, 2006, **73**, 155427.
- C. Majumder, A. K. Kandalam and P. Jena, *Phys. Rev. B*, 2006, **74**, 205437.
- K. Koyasu, Y. Naono, M. Akutsu, M. Mitsui and A. Nakajima, *Chem. Phys. Lett.*, 2006, **422**, 62.
- C. Majumder, *Phys. Rev. B*, 2007, **75**, 235409.
- L. M. Wang, R. Pal, W. Huang, X. C. Zeng and L. S. Wang, *J. Chem. Phys.*, 2010, **132**, 114306.
- X. Li, B. Kiran, L. F. Cui and L. S. Wang, *Phys. Rev. Lett.*, 2005, **95**, 253401.
- T. Höltzl, P. Lievens, T. Veszprémi and M. T. Nguyen, *J. Phys. Chem. C*, 2009, **113**, 21016.
- L. Lin, T. Höltzl, P. Gruene, P. Claes, G. Meijer, A. Fielicke, P. Lievens and M. T. Nguyen, *ChemPhysChem*, 2008, **9**, 2471.
- L. Lin, P. Claes, P. Gruene, G. Meijer, A. Fielicke, P. Lievens and M. T. Nguyen, *ChemPhysChem*, 2010, **11**, 1932.
- W. Bouwen, F. Vanhoutte, F. Despa, S. Bouckaert, S. Neukermans, L. T. Kuhn, H. Weidele, P. Lievens and R. E. Silverans, *Chem. Phys. Lett.*, 1999, **314**, 227.
- N. Veldeman, E. Janssens, K. Hansen, J. De Haec, R. E. Silverans and P. Lievens, *Faraday Discuss.*, 2008, **138**, 147.
- D. J. Goebbert, G. Meijer and K. R. Asmis, *AIP Conf. Proc.*, 2008, **1104**, 22.
- D. J. Goebbert, T. Wende, R. Bergmann, G. Meijer and K. R. Asmis, *J. Phys. Chem. A*, 2009, **113**, 5874.
- D. Oepts, A. F. G. van der Meer and P. W. van Amersfoort, *Infrared Phys. Technol.*, 1995, **36**, 297.
- E. Janssens, G. Santambrogio, M. Brümmer, L. Wöste, P. Lievens, J. Sauer, G. Meijer and K. R. Asmis, *Phys. Rev. Lett.*, 2006, **96**, 233401.
- M. Brümmer, C. Kaposta, G. Santambrogio and K. R. Asmis, *J. Chem. Phys.*, 2003, **119**, 12700.
- K. R. Asmis and J. Sauer, *Mass Spectrom. Rev.*, 2007, **26**, 542.
- M. J. Frisch, G. W. Trucks, H. B. Schlegel and co-workers. *GAUSSIAN 03, Revision A.1*, Gaussian, Inc., Pittsburgh, PA, 2003.
- A. D. Becke, *Phys. Rev. A*, 1988, **38**, 3098.
- J. P. Perdew, *Phys. Rev. B*, 1986, **33**, 8822.
- K. A. Peterson and C. Pizzarini, *Theor. Chem. Acc.*, 2005, **114**, 283.

- 39 K. A. Peterson, D. Figgen, M. Dolg and H. Stoll, *J. Chem. Phys.*, 2007, **126**, 124101.
- 40 K. A. Peterson, D. Figgen, E. Goll, H. Stoll and M. Dolg, *J. Chem. Phys.*, 2003, **119**, 11113.
- 41 M. Kohout, F. R. Wagner and Y. Grin, *Int. J. Quantum Chem.*, 2006, **106**, 1499.
- 42 Electron localization indicator has two nonequivalent definitions due to the mathematical interchangeability of the electron density and the same-spin pair density in the derivation. For details, see ref. 38. Here we always use the ELI-D function.
- 43 M. Kohout, *program DGrid, version4.1*, Max-Planck Institut für Chemische Physik und Fester Stoffe, Dresden, 2006.
- 44 E. D. Glendenning, J. K. Badenhoop, A. E. Reed, J. E. Carpenter, J. A. Bohmann, C. M. Morales and F. Weinhold, *NBO5.G*, Theoretical Chemistry Institute, University of Wisconsin, Madison, WI, 2001.
- 45 A. L. Tenderholt, Pymolyze, Version 1.1, <http://pymolyze.sourceforge.net>.
- 46 T. Höltzl, N. Veldeman, T. Veszprémi, P. Lievens and M. T. Nguyen, *Chem. Phys. Lett.*, 2009, **469**, 304.
- 47 K. R. Asmis and J. Sauer, *Mass Spectrom. Rev.*, 2007, **26**, 542.
- 48 E. Janssens, S. Neukermans and P. Lievens, *Curr. Opin. Solid State Mater. Sci.*, 2004, **8**, 185.
- 49 W. A. de Heer, *Rev. Mod. Phys.*, 1993, **65**, 611.
- 50 E. Janssens, H. Tanaka, S. Neukermans, R. E. Silverans and P. Lievens, *New J. Phys.*, 2003, **5**, 46.
- 51 K. Clemenger, *Phys. Rev. B*, 1985, **32**, 1359.